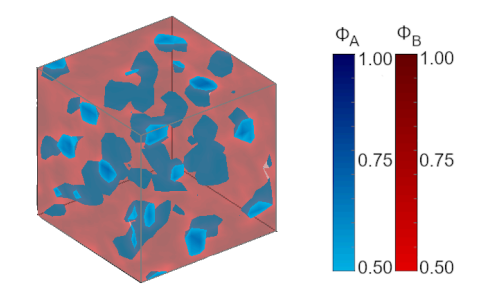
# The disordered micelle regime in a conformationally asymmetric diblock copolymer melt

Guo Kang Cheong and Kevin D. Dorfman\*

Department of Chemical Engineering and Materials Science, University of Minnesota –

Twin Cities, 421 Washington Ave SE, Minneapolis, MN 55455 USA

E-mail: dorfman@umn.edu



### Abstract

We report results from Monte-Carlo Field Theoretic Simulations (MC-FTS) of a compositionally asymmetric diblock copolymer melt ( $f_A = 0.2$ ) at an invariant degree of polymerization of  $\bar{N} = 10^4$  for both a conformationally symmetric system, where the statistical segment lengths are equal, and a high statistical segment length ratio of  $\epsilon = 3$  that promotes the formation of Frank-Kasper phases. For this conformationally symmetric system, the disordered micelle regime emerges near the order-disorder transition predicted by self-consistent field theory (SCFT), consistent with theory and

<sup>\*</sup>To whom correspondence should be addressed

recent observations from molecular dynamics simulations of a related system. The disordered micelle regime is associated with a sharp increase in the number of micellar particles per unit volume, which need to fuse to reach the particle density required to form an ordered body-centered cubic (bcc) state past the order-disorder transition. The addition of conformational asymmetry for this system does not significantly impact the location of the order-disorder transition, but it raises the SCFT order-disorder transition to a higher segregation strength. As a result, the disordered micelle regime is suppressed, with the number density of particles rising monotonically to the bcc number density. If this tentative conclusion about the role of conformational asymmetry obtained from observations for a single system proves to be valid in general, it suggests that thermal processing routes towards Laves phases in particle-forming diblock copolymer melts, which presumably require access to a disordered micelle regime, must operate at low invariant degrees of polymerization to realize a sufficiently wide disordered micelle regime.

# Introduction

Diblock copolymers with a high degree of compositional asymmetry produce (approximately) spherical particles with the minority A-block partitioning to the core of the spheres, which pack onto a lattice at low temperatures with the majority B-block forming the matrix. For conformationally symmetric systems, where the statistical segment lengths  $b_{\rm A}$  and  $b_{\rm B}$  are equal, a single particle type is formed which packs on a bcc lattice, with the exception of a narrow region of close packing near the order-disorder transition. Feaking the conformational symmetry such that the matrix blocks are stiffer than the core blocks leads to the emergence of the tetrahedrally close-packed Frank-Kasper hases  $\sigma$ , has  $\sigma$ , have  $\sigma$  and C15, have  $\sigma$  and C15, have  $\sigma$  provided that the conformational asymmetry is sufficiently large such that the imprinting of the Voronoi cells onto the A/B interface favors more spherical micellar particles. Frank-Kasper phases have large unit cells and comprise multiple

particle types with 12-fold, 14-fold, 15-fold or 16-fold coordination. The emergence of such low-symmetry phases in block polymer melts has spurred significant interest since the initial report of a  $\sigma$  phase in 2010.<sup>7</sup>

In SCFT, the linear diblock copolymer melt phase diagram is described by three parameters: (i) the volume fraction of the minority block  $f_A$ , which quantifies the degree of compositional asymmetry; (ii) the Flory Huggins parameter  $\chi N$  with N being the degree of polymerization, which quantifies the segregation strength between the blocks; and (iii) the conformational asymmetry  $\epsilon = b_{\rm A}/b_{\rm B}$ . An important outcome of SCFT calculations for Frank-Kasper phase formation was the recognition that conformational asymmetry  $\epsilon > 1$  is a necessary but not sufficient condition. <sup>18–20</sup> Explicitly, the formation of Frank-Kasper phases is favored over bcc in the polyhedral interface limit, where the geometry of the Wigner-Seitz cells is imposed on the AB interface, <sup>20</sup> because the particles in Frank-Kasper phases are more spherical on average than bcc<sup>8</sup> and represent a better compromise between chain stretching and interfacial tension. <sup>21</sup> Conformational asymmetry aids in imprinting because it penalizes stretching of matrix chains, <sup>22,23</sup> thereby promoting the formation of Frank-Kasper phases. Conformational asymmetry also produces a right-skew in the phase diagram <sup>24</sup> that stabilizes particle-forming phases to larger values of  $f_A$ , which again favors imprinting and allows Frank-Kasper phases to overtake bcc as  $f_A$  increases before the onset of the hexagonal cylinder phase. 19 However, SCFT is only valid in the mean-field limit where compositional fluctuations are suppressed. The extent that fluctuations play a role is captured by a fourth parameter, the invariant degree of polymerization  $\bar{N}=b_{\rm eff}^6\rho_0^2N,$  where  $b_{\rm eff}^2=f_{\rm A}b_A^2+(1-f_{\rm A})b_{\rm B}^2$ is the effective statistical segment length and  $\rho_0$  is the bulk monomer volume density. <sup>25</sup>

There are already three key pieces of evidence that the fluctuation effects emerging at finite  $\bar{N}$  are important for Frank-Kasper phase formation. First, Bates *et al.*<sup>10</sup> showed that fluctuations stabilize the A15 phase over the  $\sigma$  phase in a system with very high conformational asymmetry ( $\epsilon = 1.85$ ) at  $f_{\rm A} = 0.3$ , rectifying an apparent disagreement between experimental data and SCFT. Second, Lewis *et al.*,<sup>26</sup> using a poly(styrene)-*b*-poly(1,4-butadiene)

system with  $\epsilon = 1.30$  similar to the poly(ethylethylene)-b-poly(lactide) system system produced a wide Frank-Kasper phase window at  $\bar{N}_b \approx 80$  in the work of Schulze et al., <sup>13</sup> found no Frank-Kasper phases at  $\bar{N}_b = 800$ . In the latter,  $\bar{N}_b$  refers to the average invariant degree of polymerization of each block; the total  $\bar{N}$  values used by Lewis et al. 26 ranged from 1100-1400. Lewis et al. 26 proposed that Frank-Kasper phases are suppressed when  $\bar{N}_{\rm b}$  exceeds a crossover value of approximately 400 and connected that behavior to an analogy with entanglement dynamics. Third, and most relevant to our motivation here, thermal processing across the ODT has found remarkable success in coaxing the formation of Frank-Kasper phases in regions of phase diagram where they are unlikely to be the stable state.  $^{9,16}$  In one example, Kim  $et\ al.^{16}$  rapidly cooled their diblock copolymer samples in liquid nitrogen and discovered the formation of C14 phase by annealing at temperatures where bcc is usually found. In a subsequent study, Kim  $et\ al.^{17}$  postulated that long-lived non-equilibrium structures in the disordered liquid states of the micelles above the order-disorder temperature,  $T_{\rm ODT}$ , are kinetically trapped by the rapid cooling procedure. These structures subsequently guide the formation of the observed metastable states, which remarkably persist over multiple cooling and heating cycles across  $T_{\rm ODT}$ . This idea is attractive considering the observation of liquid-like packing (LLP) structures after rapid cooling, which potentially retains the favorable micelle size distribution for the reformation of the metastable state. <sup>16</sup> The formation of a dodecagonal quasicrystalline state (DDQC) following rapid cooling, which eventually reorders into the  $\sigma$  phase, might be a manifestation of the same phenomena. Indeed, DDQC can be tiled with the same building blocks as the  $\sigma$  phase, analogous to the speculation that capturing the structure of the disordered liquid state guides the formation of C14 and C15. 9

In all of these cases, the emergence of Frank-Kasper phases could have intrinsic ties to structure present in the disordered micelle state, in particular for thermal processing pathways. The window of the disordered micelle state should increase as  $\bar{N}$  decreases, <sup>27</sup> which may be one of the factors promoting Frank-Kasper phase formation at low  $\bar{N}$ ; a wide window of disordered micelles could support long-lasting disordered structures, which are then able

to transition into Frank-Kasper phases below  $T_{\rm ODT}$ . <sup>16,17</sup> To understand such phenomena, it is necessary to understand first the region of state space where disordered micelles arise under the influence of both composition fluctuations and conformational asymmetry. While molecular dynamics simulations <sup>28</sup> have successfully quantified the structure factor of the disordered state over a large range of compositions for compositionally asymmetric diblock copolymers with  $\epsilon = 1$ , no study of the disordered phase exists that addresses the effects of conformational asymmetry in the particle-forming limit for a finite  $\bar{N}$  diblock copolymer. We begin to address this issue here through an examination of the impact of conformational asymmetry on a compositionally asymmetric system ( $f_{\rm A}=0.2$ ) at  $\bar{N}=10^4$ .

### Methods

Monte-Carlo Field Theoretic Simulation (MC-FTS) is a framework to study composition fluctuations in incompressible diblock copolymer melts, <sup>29–34</sup> and thus amenable to our goal of understanding how conformational asymmetry affects the disordered micelle state. Unlike particle-based methods such as molecular dynamics simulations, the computational time of field-based methods such as MC-FTS decreases with increasing chain length, <sup>35</sup> and recent advances have enabled simulations of chain lengths near experimentally relevant molecular weights. <sup>31</sup> We chose to use MC-FTS over complex Langevin simulations, <sup>36,37</sup> an alternative field-based method that incorporates both compositional and pressure field fluctuations, because MC-FTS only requires a straightforward Metropolis Monte Carlo algorithm that we were able to implement as a wrapper around a modified version of our open-source GPU-accelerated implementation of SCFT. <sup>38</sup>

Our implementation of MC-FTS follows closely that of Stasiak and Matsen.  $^{30}$  The partition function in MC-FTS is based upon the Gaussian chain model,  $^{35}$ 

$$Z \sim \int \exp\left(\frac{H[W_-, w_+]}{k_B T}\right) DW_- \tag{1}$$

whose Hamiltonian, H, is governed by a fluctuating composition field  $W_{-}$  and the mean-field pressure field  $w_{+}$ , with  $k_{B}$  being Boltzmann's constant and T the temperature. The intensive Hamiltonian for a system of n chains is

$$\frac{H[W_{-}, w_{+}]}{nk_{B}T} = -\ln Q + \frac{1}{V} \int \left(\frac{W_{-}^{2}(\mathbf{r})}{\chi N} - w_{+}(\mathbf{r})\right) d\mathbf{r}.$$
 (2)

where  $n = V \rho_0/N$  is the number of chains with degree of polymerization N and density  $\rho_0$  in the system volume V. The single chain partition function,  $Q[w_+ + W_-, w_+ - W_-] \equiv Q[W_A, W_B]$ , is a functional of both fields and computed by the quadrature

$$Q = \frac{1}{V} \int q_p(\mathbf{r}, N) d\mathbf{r} \tag{3}$$

expressed in terms of the forward propagator,  $q_p(\mathbf{r}, s)$ , evaluated at the position s along the chain at the degree of polymerization, s = N; for a diblock copolymer, we define block A to occupy  $s \in [0, f_A N]$  and B to occupy  $s \in [f_A N, N]$ . The subscript p is used to distinguish a propagator  $q_p$  from the wavevector q. The forward propagator is obtained by solving the modified diffusion equation,

$$\frac{\partial}{\partial s} q_p(\mathbf{r}, s) = \left[ \frac{b_\alpha^2 N}{6} \nabla^2 - W_\alpha(\mathbf{r}) \right] q_p(\mathbf{r}, s) \tag{4}$$

where  $\alpha$  is monomer type corresponding to the current location s along the chain,  $W_{\alpha}$  is the composition field corresponding to monomer  $\alpha = \{A, B\}$ , and  $b_{\alpha}$  is the corresponding statistical segment length. The inverse propagator,  $q_p^{\dagger}(\mathbf{r}, s)$ , is obtained by solving Eq. 4 with time reversed. The forward and inverse propagators are solved with the initial condition  $q_p(\mathbf{r}, 0) = q_p^{\dagger}(\mathbf{r}, N) = 1$ . The density fraction of each monomer type  $\alpha$  is obtained from the quadrature

$$\phi_{\alpha}(\mathbf{r}) = \frac{1}{NQ} \int_{\alpha} q_p(\mathbf{r}, s) q_p^{\dagger}(\mathbf{r}, s) ds$$
 (5)

where the bounds of the integral are given by the contour positions of the block corresponding

to the monomer  $\alpha$ .

The solution of the modified diffusion equation was obtained pseudo-spectrally, and Anderson mixing<sup>39</sup> was used to modify  $w_+$  to obtain the corresponding extremum pressure field for the given composition field  $W_-$ . In MC-FTS, the definition of the deviation in Anderson mixing constrains the system to satisfy the condition of incompressibility,<sup>32</sup> i.e.  $\rho_A(\mathbf{r}) + \rho_B(\mathbf{r}) = \rho_0$  with  $\phi_\alpha(\mathbf{r})$  defined as  $\rho_\alpha(\mathbf{r})/\rho_0$ , where  $\rho_\alpha(\mathbf{r})$  is the local  $\alpha$ -monomer density.

MC-FTS evaluates the pressure field at its extremum while allowing the composition field to fluctuate. These fluctuations are sampled using a standard Metropolis Monte Carlo algorithm. Moves in the composition field are accepted by computing the change in the Hamiltonian,

$$\Delta H = H[W_{-} + \Delta W_{-}, w_{+} + \Delta w_{+}] - H[W_{-}, w_{+}]$$
(6)

and then setting the probability of acceptance for a given move of  $\Delta W_{-}$  as min(1, exp[ $-\Delta H/k_BT$ ]). Note that the extensive Hamiltonian is used for the Monte Carlo acceptance criterion in Eq. 6, rather than the intensive form given by Eq. 2. At each Monte Carlo step, two different types of moves are performed alternately.<sup>30</sup> The first type is a real space move chosen from a uniform distribution  $\Delta W_{-}(\mathbf{r}) \in [-A_1, A_1]$  at each grid point. The second move is a collective move in Fourier space,  $\Delta W_{-}(q) \in [-A_2[S_{\rm FH}(q)]^{1/2}, A_2[S_{\rm FH}(q)]^{1/2}]$  with  $S_{\rm FH}(q)$  being the Fredrickson-Helfand structure factor,<sup>25</sup> as suggested in previous work for accelerating sampling rate.<sup>30</sup> Both  $A_1$  and  $A_2$  are constants chosen to maintain about 40% acceptance rate (Supporting Information Table S1), and need to be tuned for a given system.

As a fluctuating field theory, the value of  $\chi N$  in MC-FTS has to account for the ultraviolet divergence effect present in finite  $\bar{N}$  systems.  $^{30,31,37,40,41}$  We define  $\chi N_{\rm bare}$  as the input parameter to MC-FTS and  $\chi N$  as the effective interaction parameter that is used in

comparison to theory and experiment. We use the definition from Vorselaars et al., 31

$$\chi N = \left[ 1 - \ell \frac{R_0^2 \int S_{\text{RPA},0}(q,\epsilon) d\mathbf{q}}{(2\pi)^3 \rho_0 N f_A (1 - f_A)} \right] \chi N_{\text{bare}}$$
 (7)

where  $S_{\text{RPA},0}(q,\epsilon)$  is the athermal random phase approximation (RPA) structure factor at a given value of  $\epsilon^{42,43}$  and  $\ell = R_0 \bar{N}^{-1/2}$  where  $R_0 = N^{1/2}b$  is the end-to-end length of the polymer chain. We chose this definition of  $\chi N$  since those authors<sup>31</sup> have shown that it is effective at culling the ultraviolet divergence for low  $\bar{N}$  diblock copolymers.

Our implementation of MC-FTS ran for at least  $5 \times 10^5$  iterations to first equilibrate the system and was followed by  $3.5 \times 10^6$  iterations to obtain the relevant statistics. Statistics are sampled every 10<sup>3</sup> iterations. To ensure the correctness of our implementation of MC-FTS, we repeated the calculations in Ref. 31 for the structure factor of a compositionally symmetric system and found negligible difference in the results (Supporting Information Fig. S-1). Our simulations are performed with a grid size of 16 x 16 x 16, which provides sufficient resolution to the system while maintaining a reasonable computational time. Simulations starting from a homogeneous initial state used a cubic box with length L=4, where all box sizes reported here are made dimensionless with  $N^{1/2}b_{\rm B}$ ; the latter is the end-to-end distance for the  $\epsilon=1$ system but only 62% of that for the  $\epsilon = 3$  system wherein  $b_{\rm eff} = 1.61 b_{\rm B}$ . The choice of L = 4maintains a constant spacial resolution on the grid between different simulations, which is desirable, but it can lead to incommensurability effects since  $q^*$  varies with  $\epsilon$  and  $\chi N$ , which is undesirable and likely to be a larger issue than the spatial resolution. We will return to this point in the discussion of our results to estimate the impact of this choice of a fixed L on our results. Simulations starting from the ordered state used m copies of the bcc structure that best maximize the commensurability between the unit cell size L=4 and the optimal bcc unit cell size computed SCFT. The SCFT result at  $\chi N=25$ , corresponding to L=1.86for  $\epsilon = 1$  and L = 3.61 for  $\epsilon = 3$ , was used to select m since it is the midpoint of the  $\chi N$  range used for the MC-FTS runs. We thus used a single copy of bcc at  $\epsilon = 3$  and initialized the calculations at  $\epsilon = 1$  using a  $2 \times 2 \times 2$  bcc structure.

For our analysis, we focus on the modest degree of conformational asymmetry corresponding to  $f_{\rm A}=0.2$  as a model system. Experiments on 1,4-poly(isoprene)-b-poly( $\pm$  lactide) diblock melts ( $\epsilon=1.15$ ) at this composition produced C15,  $\sigma$ , LLP or hexagonally packed cylinders depending on thermal processing route, <sup>16</sup> making this degree of compositional asymmetry relevant to Frank-Kasper phase formation. All simulations were performed at  $\bar{N}=10^4$ , which is a relatively low value of  $\bar{N}$  for a field theoretic simulation <sup>31</sup> and thus emphasizes the role of fluctuations. For the conformationally asymmetric system, we used the value  $\epsilon=3$  appearing in the work of Bates et al., <sup>10</sup> where fluctuation effects were important to the selection of the ordered state, and we use the conformationally symmetric case  $\epsilon=1$  as a control system to isolate the effects of conformational asymmetry.

Calculations were performed at the Flory-Huggins parameters  $\chi N = \{10, 20, 23, 24, 25, 26, 30\}$ , starting from either a homogeneous initial condition or a bcc state. The structure factor was computed via

$$\frac{S(\mathbf{q})}{\rho_0 N} = \frac{n}{\left(V \chi N_{\text{bare}}\right)^2} \langle W_{-}(\mathbf{q}) W_{-}(-\mathbf{q}) \rangle - \frac{1}{2 \chi N_{\text{bare}}}$$
(8)

where the ensemble average  $\langle W_{-}(\mathbf{q})W_{-}(-\mathbf{q})\rangle$  is obtained by sampling the composition field using MC-FTS.<sup>30</sup> Since we anticipate that the disordered state is an isotropic liquid, the average structure factor, S(q), is obtained by further averaging  $S(\mathbf{q})$  for each wavevector of the same magnitude in wavenumber. The simulated structure factor is directly related to the intensity profile resulting from small angle X-ray scattering experiments.<sup>44</sup>

# Results

Figure 1 provides illustrative results for the structure factor obtained at three different  $\chi N$  values for the conformationally symmetric system  $\epsilon = 1$  using bcc as the initial condition. The dashed lines are the RPA predictions<sup>42</sup> while the solid lines in Figs. 1a and b are fits to

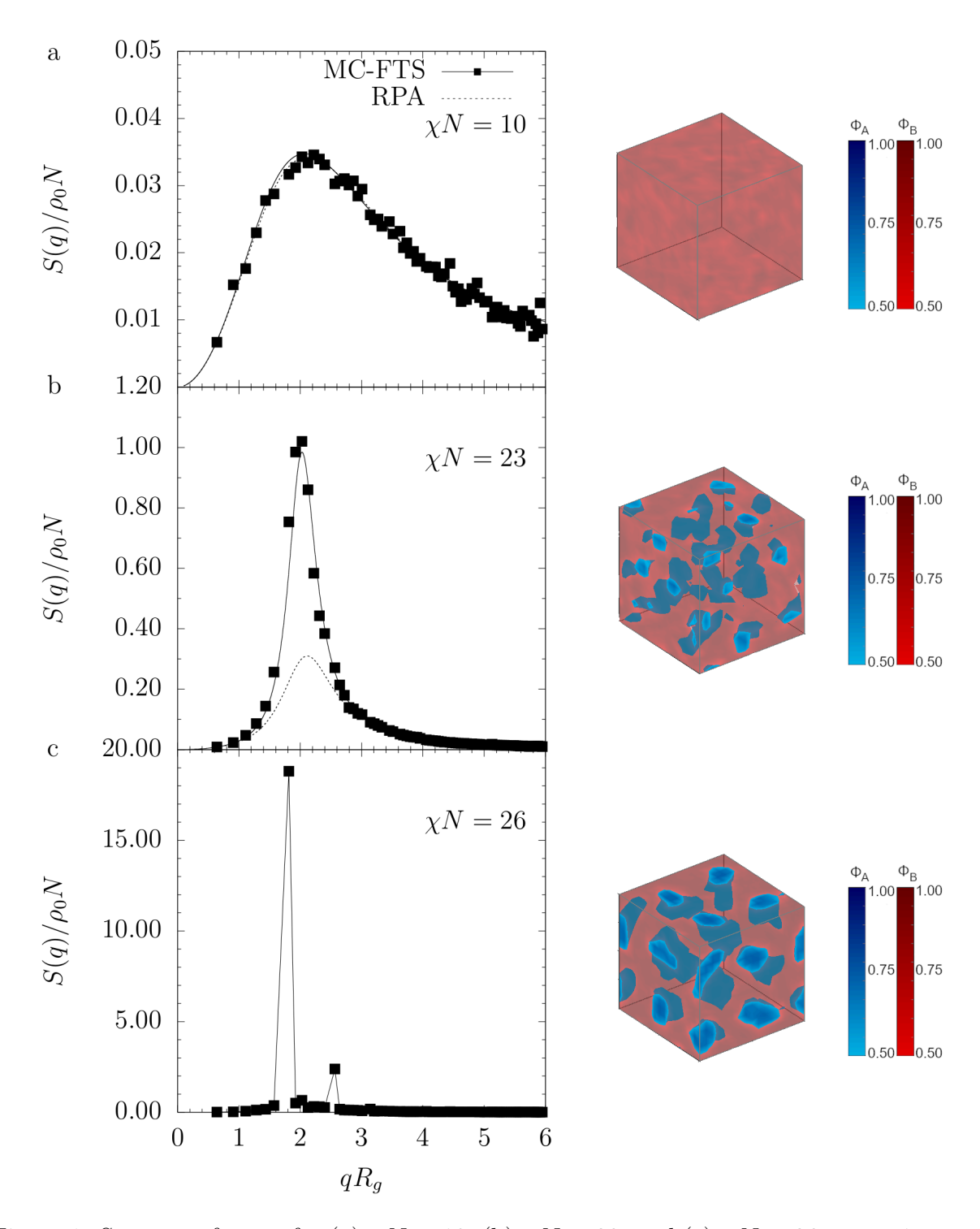


Figure 1: Structure factors for (a)  $\chi N=10$ , (b)  $\chi N=23$ , and (c)  $\chi N=26$  at  $\epsilon=1$ , started from an ordered bcc initial condition. The right column shows the corresponding density field at the particular  $\chi N$ . The solid lines in (a) and (b) are obtained from fitting to the modified RPA given in Eq. 9, while the solid line in (c) is a guide to the eye.

the modified RPA, <sup>28</sup>

$$S^{-1}(qR_g) = S_{\text{RPA}}^{-1}(qR_g, \chi N, \epsilon) + a + b(qR_g)^2 + c(qR_g)^4$$
(9)

where a, b, and c are fitting parameters. The best fit parameters are tabulated in Supporting Information Table S-2 using fittings over the  $qR_g$  ranges in Supporting Information Table S-3. Snapshots of the density field at each value of  $\chi N$  are provided with the corresponding structure factors.

At the lowest value  $\chi N = 10$ , the bcc structure melts and, subsequently, there is very little difference between the structure factor obtained by MC-FTS and the RPA prediction. <sup>43</sup> This conclusion from S(q) is further supported by visualization of the density field in the corresponding simulation snapshot. The system is not homogeneous, as would be the case in the mean-field of SCFT, but the compositional fluctuations are small. The relative agreement between the simulations and the RPA prediction suggests that the box size L=4 is sufficiently large to capture the fluctuation effects in the weakly disordered state. At  $\chi N=$ 23, the ordering in the bcc structure of the initial condition is lost but micelles remain in the system after melting. The magnitude of the resulting structure factor increases substantially compared to that at  $\chi N = 10$ , leading to a strong deviation from the RPA prediction. The qualitative behavior in Fig. 1b is consistent with previous work by Wang et al., 27 who demonstrated that the structure factor from a simulation with disordered micelles produces a larger structure factor peak intensity compared to RPA in conjunction with a left shift of the peak location to smaller  $qR_g$  values as compared to the RPA prediction. At an even higher value of  $\chi N = 26$ , a system initialized in the bcc state does not melt but undergoes fluctuations due to the finite  $\bar{N}$ . This behavior produces Bragg peaks in the structure factor, which has increased substantially in magnitude compared to its value at  $\chi N = 23$ . The bcc structure persists throughout the simulation, indicating that  $\chi N = 26$  is, at worst, a lower bound for the ODT.

Recently, Chawla et al.<sup>45</sup> used coarse-grained molecular dynamics simulations to show that the onset of disordered micelles in the sphere-forming region of the diblock copolymer phase diagram occurs at the SCFT order-disorder transition, as anticipated by theory. <sup>27,46</sup> Their simulations correspond to a conformationally symmetric system at a different compositional asymmetry ( $f_A = 0.125$ ), as well as a lower invariant degree of polymerization ( $\bar{N} = 3800$ ) that is more amenable to a particle-based simulation. For our system, SCFT calculations predict an ODT at  $\chi N = 21.55$  (see Supporting Information Fig. S-2); the appearance of disordered micelles at  $\chi N = 23$  is consistent with the observations of Chawla et al.<sup>45</sup> Our results were obtained using a different simulation method at different parameters but reach the same qualitative conclusion, providing further evidence that the critical micelle temperature (CMT) is connected to the SCFT order-disorder transition. <sup>27,45,46</sup>

Figure 2 provides the companion data to Fig. 1 for the conformationally asymmetric case  $\epsilon=3$ . For  $\chi N=10$  in Fig. 2a, the effect of conformational asymmetry is captured by the RPA; the shift in the peak  $q^*$  to lower values of q and the reduction in the magnitude of  $S(q^*)$  are both anticipated by the RPA. <sup>42</sup> However, the behavior at  $\epsilon=3$  for  $\chi N=23$  in Fig. 2b is qualitatively different than its counterpart at  $\epsilon=1$  in Fig. 1b. For the conformationally asymmetric case, disordered micelles are observed in neither the structure factor, which only somewhat deviates from the RPA prediction, nor are they prevalent in the simulation snapshot. This observation is consistent with prior work <sup>27,45,46</sup> because SCFT calculations at  $\epsilon=3$  have an ODT at  $\chi N=24.23$  (see Supporting Information Fig. S-2). When we increase the segregation strength to  $\chi N=26$  in Fig. 2c, we recover a congruence between the conformationally symmetric and asymmetric cases. Similar to the case in Fig. 1c, starting from a bcc state for  $\epsilon=3$  leads to the persistence of this state throughout the simulation.

To further understand the lack of a disordered micelle regime for the conformationally asymmetric case — and its appearance at  $\epsilon = 1$  — we computed the hysteresis loop to estimate the location of the ODT at  $\bar{N} = 10^4$  in a box with L = 4. We thus ran MC-FTS simulations starting from a homogeneous state to identify the value of  $\chi N$  that leads to

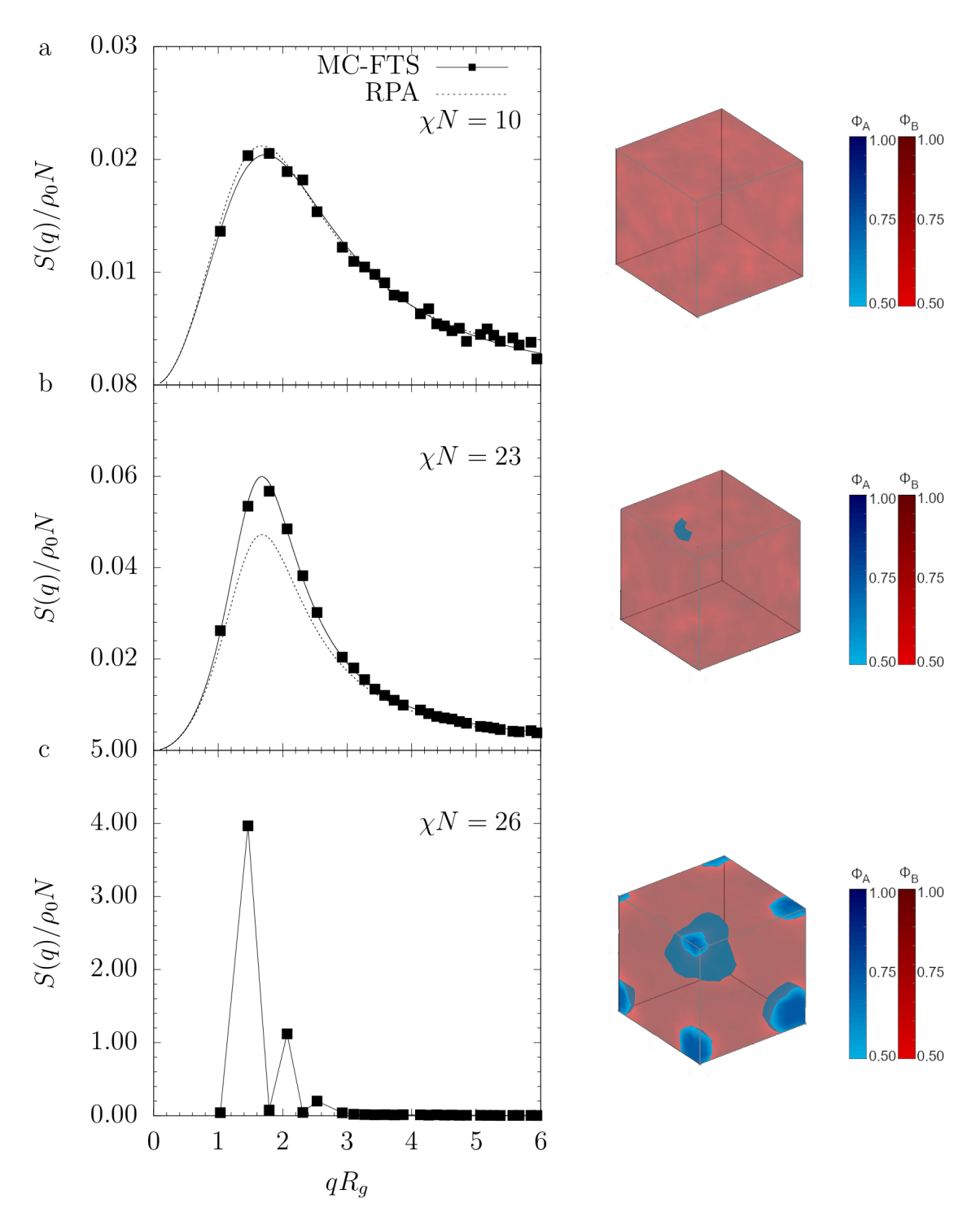


Figure 2: Structure factors for (a)  $\chi N = 10$ , (b)  $\chi N = 23$ , and (c)  $\chi N = 26$  at  $\epsilon = 3$ , started from an ordered bcc initial condition. The right column shows the corresponding density field at the particular  $\chi N$ . The solid lines in (a) and (b) are obtained from fitting to the modified RPA equation while the solid line in (c) is a guide to the eye.

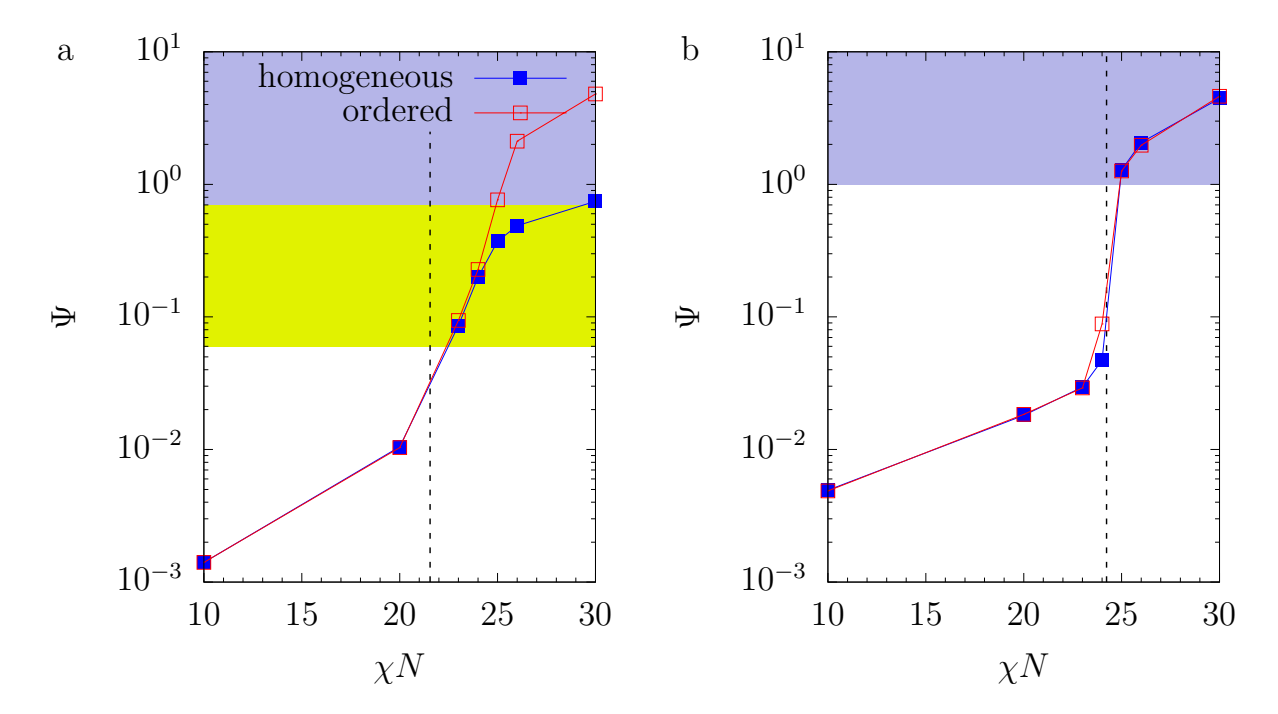


Figure 3: Order parameter,  $\Psi$ , in Eq. 10 as a function of the Flory-Huggins parameter  $\chi N$  for (a)  $\epsilon = 1$  and (b)  $\epsilon = 3$ . The solid symbols correspond to the cooling branch, where the initial condition is a homogeneous structure. Open symbols correspond to the melting branch, where the initial condition is a bcc ordered structure. The broken vertical line indicates the location of the SCFT order-disorder transition. The region where we observe the formation of the disordered micelle regime is shaded yellow, whereas the region for the formation of ordered structure is shaded blue.

the formation of an ordered bcc state, and companion simulations starting from an ordered bcc state to identity when the system melts. Six of these simulations have already been reported in Figs. 1 and 2; structure factors obtained at the other values of  $\chi N$  and initial conditions are reported in Supporting Information Figs. S-3 to S-8. We then computed the order parameter  $\Psi$  using the approach from Stasiak and Matsen, <sup>30</sup>

$$\Psi = \frac{1}{V^2} \max_{q} \langle W_{-}(q)W_{-}(-q)\rangle \tag{10}$$

computed over the wavenumbers available from the grid.

Figure 3 provides the resulting hysteresis curves for the conformationally symmetric case (a) and the conformationally asymmetric case (b). For both cases, we find that  $\Psi$  is es-

sentially independent of the initial condition up to  $\chi N=23$ . For the conformationally symmetric case, Fig. 1b shows that  $\chi N=23$  corresponds to the onset of the disordered micelle regime above the SCFT order-disorder transition, whereas Fig. 2b shows that the behavior for  $\chi N=23$ , which is below the SCFT order-disorder transition at  $\epsilon=3$ , remains in a disordered state without the formation of micelles. As  $\chi N$  increases further, the hysteresis loops for the two cases differ. For  $\epsilon=1$ , there is a small difference between the heating and cooling curves at  $\chi N=24$  but then the system fails to form a bcc structure at higher  $\chi N$ . In contrast, for  $\epsilon=3$ , we observe a somewhat larger deviation between the two branches at  $\chi N=24$  but the hysteresis loop closes at  $\chi N=25$ .

The differing behavior in Fig. 3 for  $\epsilon = 1$  and  $\epsilon = 3$  at the highest values of  $\chi N$  can be attributed to box-size effects. All of the simulations were performed in a cubic box with length L=4. For  $\epsilon=1$ , the box is large enough to fit eight copies of the bcc unit cell. As noted by Beardsley and Matsen, <sup>34</sup> the cooling branch of the system in a large unit cell, such as that used in our calculations, is prone to defect formation during crystallization. Simulation snapshots for  $\epsilon = 1$  (Supporting Information Fig. S-4) suggest that the system is indeed defective, leading to large differences in the structure factor for wavevectors  $\mathbf{q}$  that have the same magnitude q (Supporting Information Fig. S-9). It is also possible that the increase in the free energy of the ordered state via unit cell strain caused by the incommensurate box is hindering the formation of the ordered state. Owing to the ease of defect formation during crystallization, Beardsley and Matsen<sup>34</sup> recommended using the melting branch of the hysteresis loop as the estimate for the ODT, which we will do here for  $\epsilon = 1$ . For  $\epsilon = 3$ , the box size is relatively close to the SCFT unit cell size and we did not observe any issues with forming the bcc phase from either simulation snapshots (Supporting Information Fig. S-6) or the structure factor for planes with equivalent values of q (Supporting Information Fig. S-10). To confirm these observations from cooling at L=4, we confirmed that the  $\epsilon$ = 1 system will crystallize under MC-FTS when run in a box size of L=1.86 at  $\chi N=$ 26 and 30 (Supporting Information Fig. S-11). The ability to crystallize both the  $\epsilon = 1$  and  $\epsilon = 3$  systems in single unit-cell systems may be connected the the inability of such a small system to make a fluid if it only forms two micelles. We also confirmed that the  $\epsilon = 3$  system does not melt at  $\chi N = 25$ , 26 and 30 when run in a box size L = 7.22 that can fit eight copies of bcc (Supporting Information Fig. S-12). While it is possible to repeat all of the results for  $\epsilon = 1$  in a smaller box size to produce a tighter hysteresis loop, we will adopt the approach of Beardsley and Matsen<sup>34</sup> and use the melting branch to estimate the order-disorder transition, making those additional costly calculations, which may also suffer from finite-size effects, superfluous.

For the conformationally symmetric case  $\epsilon = 1$ , the fluctuations cause the ODT to shift from the SCFT prediction by  $\Delta \chi N = 3.45$ , which is similar to the shift  $\Delta \chi N = 3.04$  observed for  $f_{\rm A} = 0.25$  when the ODT obtained from those molecular dynamics simulations <sup>47</sup> is extrapolated to  $\bar{N} = 10^4$ . There is a negligible shift in the ODT for the conformationally asymmetric system  $\epsilon = 3$ , leading us to conclude that the ODT at  $f_{\rm A}$  and  $\bar{N} = 10^4$  is not affected appreciably by conformational asymmetry to within the limitations noted in the previous paragraph.

In addition to the reciprocal space analysis, we also analyzed the density field samples from the MC-FTS simulations using a simple breadth-first search algorithm to determine the locations of micelles. The algorithm first picks an initial position  $\mathbf{r}_0$  in the unit cell that satisfies

$$\phi_A(\mathbf{r} = \mathbf{r}_0) > I \tag{11}$$

where I is an isovalue selected to represent a concentration fluctuation above the background. We chose I = 0.60, which is sufficiently high such that the minority block is the majority component at that location. This value is also consistent with the purity of the micelle core in particle-based simulations when the system crosses the purported CMT. <sup>45</sup> The algorithm then iteratively marks adjacent grid points as part of the same micelle if they fulfill the condition in Eq. 11. The algorithm ends when every grid point is visited and, if Eq. 11 is fulfilled, clustered as part of their respective micelles.

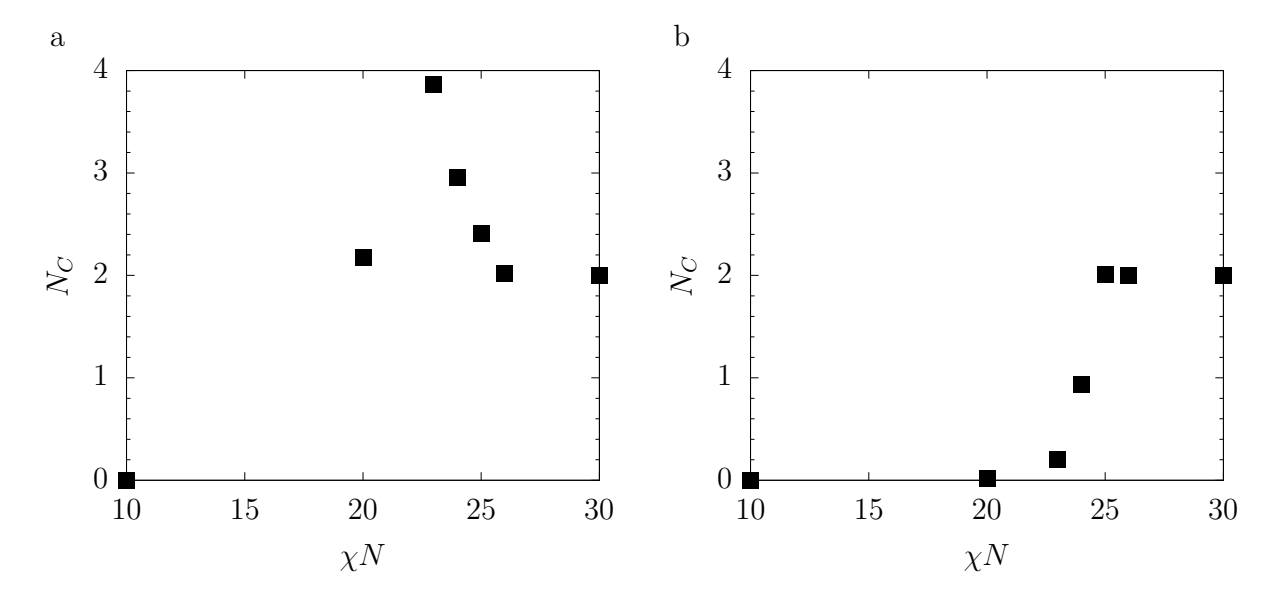


Figure 4: Average number of clusters per bcc unit cell versus segregation strength  $\chi N$  for (a)  $\epsilon = 1$  and (b)  $\epsilon = 3$  for calculations started from the ordered initial condition.

Figure 4 provides the number of micelles per bcc unit cell volume,  $N_c$ , as a function of  $\chi N$  for the conformationally symmetric case (a) and the conformationally asymmetric case (b) for calculations started from the ordered bcc state with L=4. When this ordered state persists at high  $\chi N$ , the clustering algorithm produces two particles per unit cell, as expected. Likewise, at the lowest value of  $\chi N=10$ , where the RPA approximation is a good description of the structure factor, the clustering algorithm identifies no micelles within the system since the compositional fluctuations at  $\chi N=10$  are insufficient to exceed the isovalue.

These results at the extrema in  $\chi N$  indicate that the clustering analysis is robust for those limiting cases. Nevertheless, a cluster analysis based on the volume fractions at the grid points in a field theoretic simulation is not as effective at identifying micelles when compared to a particle-based simulation. <sup>45</sup> The cluster analysis in a field theoretic simulation requires connecting contiguous regions that exceed a threshold value, which do not necessarily correspond to a set of chains that are linked by proximity of their respective segments, the latter being a relatively straightforward calculation in the particle-based simulation.

Although this shortcoming limits the definitiveness of any conclusions obtained from the real-space analysis, it is still illuminating to examine the real-space behavior, in particular to see if it is consistent with the structure factor data and whether it can provide any additional insights into the formation of a disordered micelle regime.

The number of clusters is qualitatively different for intermediate values of  $\chi N$  when the system becomes conformationally asymmetric, further supporting the conclusions drawn from Figs. 1-3. For the conformationally symmetric case, where Fig. 1 demonstrates the emergence of a disordered micelle regime, there are initially a large number of small particles that presumably undergo fusion as the system approaches the ODT, whereupon they would need to organize on the lattice. In contrast, the conformationally asymmetric system exhibits a monotonic increase in the number of particles before reaching the ODT. The appearance of approximately one particle per unit cell volume at  $\chi N=24$  for  $\epsilon=3$  suggests that there may be a very narrow region of disordered micelles proximate to the SCFT order-disorder transition at  $\chi N=24.23$ . This observation is also consistent with the snapshot in Fig. 2b, which shows the formation of a single potential micelle in that particular sample of the fields. However, the number of micelles per unit volume is much smaller than the disordered micelle regime observed at  $\epsilon=1$ , and fluctuations above the isovalue are rare. Indeed, the number of micelles for  $\epsilon=3$  near the SCFT order-disorder transition is almost half that for the  $\epsilon=1$  case, where the SCFT order-disorder transition is at  $\chi N=21.55$ .

We have also attempted to measure the average micelle sizes from the real-space analysis. Here, the volume of the micelles is determined by multiplying the number of grid points in a cluster by the volume occupied by the cube surrounding a grid point. The typical micelle size,  $R_m$ , is then obtained by taking the cube root of that volume, and thus represents an estimate of the total size of the micelle core and part of the diffuse interface since we are using grid points out to I = 0.6. For simplicity, we refer to this object as the micelle "core" in what follows.

Figure 5 furnishes the results of the computation of the micelle core size. To see if these

sizes are reasonable, recall that the vector along the close-packed [111] direction has a length  $L\sqrt{3}$  and needs to fit 4 micelles (for  $\epsilon=1$ ) and 2 micelles (for  $\epsilon=3$ ) in the ordered state. Using  $\epsilon=1$  and  $\chi N=25$  as a test case, each micelle occupies a dimensionless length  $\sqrt{3}$  along the [111] direction. From the data in Fig. 5, where  $R_m\approx 0.75$  at these conditions, the micelle core occupies approximately 43% of that distance. This result is in reasonable agreement with that predicted by SCFT in Fig. S13 in the Supporting Information, which clearly illustrates the diffuseness of the interface. Measuring the distance between values of  $\phi_A=0.6$  along the [111] direction from SCFT leads to the micelle core occupying 54% of the distance. Some of this disagreement between the MC-FTS data and SCFT is due to fluctuations captured in MC-FTS, but it also reflects the challenges in measuring precisely the micelle volume fraction using the grid clustering method compared to the relatively smooth volume fraction data produced by SCFT.

Figure 5 reveals that, as anticipated, the micelle size increases with segregation strength and that the conformationally asymmetric micelles are larger due to their larger values of  $b_A$ . For the  $\epsilon = 1$  data, the gradual increase in the micelle sizes indicates that incommensurability is becoming increasingly important as  $\chi N$  increases, since increasingly larger micelles are forced to order within the same box size. Such incommensurability could frustrate crystallization from an initially disordered system, which was noted in our discussion of the hysteresis loop in Fig. 3.

The most interesting result concerning micelle sizes in Fig. 5 is the general correspondence between the trends in micelle size here and those observed for  $\log \Psi$  in Fig. 3. The ODT inferred from the jump in  $\Psi$  for  $\epsilon = 3$  is coincident with a sharp increase in the measured size of the micelle cores in Fig. 5 and the number of such clusters in Fig. 4. Taken together, the latter observations provide real-space support our claim that the disordered micelle regime is largely suppressed in the  $\epsilon = 3$  system.

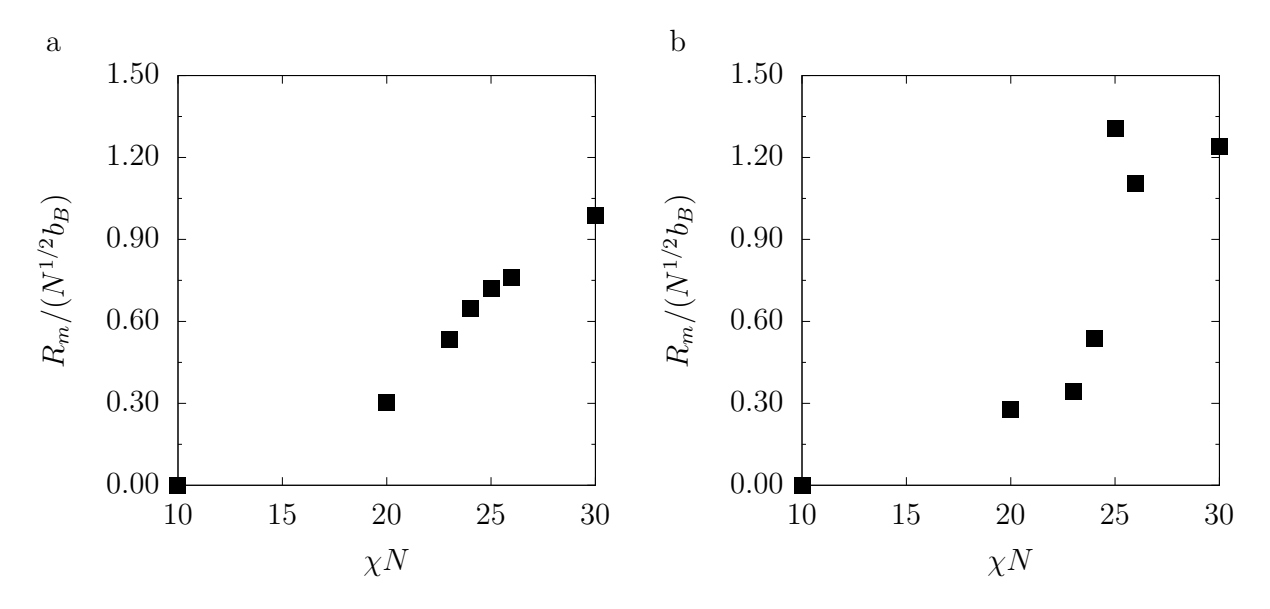


Figure 5: Average micelle size  $R_m$ , in terms of versus segregation strength  $\chi N$  for (a)  $\epsilon = 1$  and (b)  $\epsilon = 3$  for calculations started from the ordered initial condition.

### Discussion

The key results of our MC-FTS simulations of conformational asymmetry on the compositional fluctuations  $f_A$  at  $\bar{N}=10^4$  are that (i) the emergence of disordered micelles is roughly coincident with the SCFT order-disorder transition and (ii) the order-disorder transition does not appear to shift as a result of conformational asymmetry. The first conclusion is consistent with previous molecular dynamics simulations of a somewhat more compositionally asymmetric system at an even lower invariant degree of polymerization 45 and theory. 27,46 The second conclusion suggests that fluctuations are more important than conformational asymmetry in determining the ODT. Prior SCFT works on the effect of conformational asymmetry  $^{24,48}$  have suggested that conformational asymmetry has a small effect on the ODT, at least when compared to the large skew in the order-order transitions as  $\epsilon$  increases. Our SCFT conclusion is consistent with these prior studies; even when operating at a relatively large conformational asymmetry, we still only observed a modest shift in the SCFT ODT from  $\chi N = 21.55$  to  $\chi N = 24.23$ . The more interesting conclusion that we draw is that the cutoff of the lower part of the phase diagram created by fluctuation effects at  $\bar{N} = 10^4$  ap-

pears to be more important for establishing the location of the lower bound for the true ODT than the effect of conformational asymmetry, leading to an estimate of the true ODT that is seemingly independent of  $\epsilon$  for this system. We recognize that this is a tentative conclusion, drawn from results at a single value of  $f_A$  and  $\bar{N}$ , and a considerable amount of additional work is required to draw a firm conclusion. The recent advances in accelerating this class of field-theoretic simulations may render such a calculation feasible but still expensive. <sup>33,34,49</sup>

The results obtained here further emphasize the importance of finite  $\bar{N}$  on the emergence of Frank-Kasper phases, in particular for thermal processing routes that produce the C14 and C15 Laves phases. 16 As noted in the introduction, Frank-Kasper phases are predicted by SCFT to emerge at equilibrium as a consequence of conformational asymmetry,  $^{18-20}$  and thus do not require access to a disordered micelle regime to promote non-equilibrium emergence of those phases. However, only the A15 and  $\sigma$  phases appear in the equilibrium phase diagram. <sup>16</sup> Experiments on neat diblock copolymer melts have also produced the C14 and C15 Laves phases, which are expected to be metastable phases at equilibrium  $^{16}$  and thus require processing to access them as non-equilibrium, long-lived states. Presumably, the emergence of the Laves phases is connected to the structure of the disordered micelle state proximate to the ODT that can template their formation out of equilibrium via thermal processing. 17 Our analysis reveals that conformational asymmetry, which is required for the formation of a Frank-Kasper phase, raises the the onset of the disordered micelle regime, which appears to be coincident with the SCFT order-disorder transition,  $^{27,45,46}$  to a higher value of  $\chi N$ . However, for the value of  $\bar{N} = 10^4$  used here to examine the effect of compositional fluctuations, which is already on the lower end for a field-theoretic simulation, does not raise the true ODT sufficiently to expose an accessible window of  $\chi N$  for thermal processing through a disordered micelle state, keeping in mind that the melting simulation is an estimate of the lower bound for the ODT. Thus, our results suggest that the thermal processing approach to producing Laves phase requires even lower values of  $\bar{N}$ , consistent with the fact that the thermal processing experiments by Kim et~al. <sup>16,17</sup> used an even lower invariant degree of polymerization  $\bar{N} = 330$ .

Making a further connection between conformational asymmetry and the structure of the disordered state, in particular for conditions that are most relevant to thermal processing experiments, thus necessitates simulations at even lower values of  $\bar{N}$ . Such simulations are challenging using a field-theoretic model due to the increasing magnitude of the composition fluctuations as  $\bar{N}$  decreases. Recent simulations of this type by Beardsley and Matsen, <sup>34</sup> which took advantage of multiple methods for accelerating the simulations, were performed at  $\bar{N}=10^4$ , the same as the simulations appearing here. Vorselaars *et al.*<sup>31</sup> were able to perform MC-FTS simulations down to  $\bar{N}=10^3$  for compositionally symmetric systems that produce a lamellar morphology, which is promising but a simpler problem than a sphere-forming phase, especially in the context of relieving unit cell stress.

Most likely, molecular dynamics simulations of a coarse-grained polymer model are the best approach to understand the structure of the disordered state at the low values of  $\bar{N}$  used for thermal processing experiments, 16,17 as they have proven effective for interrogating the properties of conformationally symmetric disordered systems in the past. <sup>28,45,47</sup> However, one outstanding challenge in molecular dynamics simulations of this type is locating the upper bound for the ODT; similar to our results here, it is relatively easy to obtain data for the melting branch of the hysteresis loop, but these simulations seem to resist crystallization on the cooling branch. 45 Our data for cluster sizes in Fig. 4 provide an insight into the challenge of dynamically simulating the crystallization process in a particle-based model. If the number of clusters increases in the disordered micelle regime, which is the case in Fig. 4a past the SCFT order-disorder transition, then the eventual equilibration of the system into a bcc state requires changing the total number of micelles. Changes in micelle number typically require fission and fusion processes, which are very slow in a molecular dynamics simulation. <sup>50</sup> MC-FTS, like most Monte Carlo methods, does not require tracking the dynamics of the polymers and thus allows for moves in the configurational space that can equilibrate particle numbers much more quickly.

One concern in our identification of the ODT is a possible systematic error in our analysis related to the unit cell size. In both particle-based and field-based methods, the choice of unit size is especially important in determining the selection of the ordered state above the ODT. 31,47 Using an incommensurate box size leads to stress in the ordered state, 51 which increases its free energy relative to that in an optimally sized box and thus destabilizes the ordered state relative to disorder. For the  $\epsilon=3$  case, any incommensurability of the unit cell at L=4 only serves to reinforce our conclusion that the disordered micelle regime is suppressed. Acting on the assumption that the CMT is roughly coincident with the meanfield ODT predicted by SCFT, <sup>27,45,46</sup> using a MC-FTS box size that is closer to the optimal unit cell dimension would stabilize the ordered system and cause it to melt at an even higher temperature, which is equivalent to reducing the  $\chi N$  value corresponding to the true ODT. This box size effect should not affect the CMT, which is estimated from the mean-field  $\mathrm{ODT.^{27,45,46}}$  As a result, the window between the CMT and ODT would be narrower in a more commensurate box, and the key insights with respect to thermal processing experiments for the  $\epsilon = 3$  system would remain valid. However, any incommensurability for the  $\epsilon = 1$ case would overpredict the width of its disordered micelle regime in MC-FTS as well. The magnitude of this shift is uncertain, although our extrapolation from previous coarse-grained molecular dynamics studies 47 suggests that the window between the CMT, as estimated from the mean-field ODT, and the true ODT may still be as large as  $\Delta \chi N = 3$ . If this extrapolation proves to be accurate, then there would still be a substantial difference in the width of the disordered micelle regime between  $\epsilon = 1$  and  $\epsilon = 3$  in commensurate box sizes, albeit not as dramatic as that seen here from MC-FTS simulations using L=4.

The latter discussion of the role of the box size raises an important point regarding the selection of the box size L for computationally intense methods such as MC-FTS. While better estimates for L than the fixed value used here are available from the  $q^*$  values predicted by RPA (for the disordered state) and SCFT (for the ordered state), it would be very useful to have a way to relieve the unit cell stress during MC-FTS calculations, which would render

the a priori selection of L moot. For the compositional symmetric diblock copolymer case, Vorselaars et al. 31 relieved the stress on the unit cell by performing a volume-preserving, box-altering Monte Carlo move in their study of the lamellar phase. Unfortunately, this approach does not readily translate to a cubic system. The only direct method, at present, to determine the optimal cubic unit cell for our system of compositional asymmetric chains is through a computational expensive thermodynamic integration over a broad range of unit cell sizes 32 or by simulating many different box sizes. 34 Ideally, one would like to have a method similar to that used to minimize unit cell stress in SCFT 51 to adjust the box size in the field theoretic simulation.

### Conclusion

This work investigated the effects of conformational asymmetry in compositionally asymmetric diblock copolymers using MC-FTS calculations. The onset of the disordered micelle regime is marked by a strong deviation from the RPA prediction for the structure factor and an increase in the number of micelles, without any long-ranged order. For the particular case of  $f_A = 0.2$  and  $\bar{N} = 10^4$  studied here, the disordered micelle regime is suppressed in the conformationally asymmetric system due to the increase in the mean-field order-disorder transition with conformational asymmetry. This is an intriguing result related to conformational asymmetry, but was obtained from a single value of  $f_A$  and  $\bar{N}$ . If it proves to be valid in general, then this work represents a key step in further developing the understanding of the behavior of the disordered micelle phase, reinforcing prior work <sup>45</sup> on the emergence of disordered micelles at the SCFT order-disorder transition and highlighting that compositional fluctuations, which are controlled by the invariant degree of polymerization  $\bar{N}$ , may be more important for determining the ODT than conformational asymmetry. In the case where the long-lived structures in the disordered micellar states are highly correlated with the formation of different Frank-Kasper phases, <sup>16,17</sup> a comprehensive understanding of the

behavior of the disordered micelle phase should provide a deep understanding of how transitions across the order-disorder transition impact the selection of complex sphere-forming phases.

### Acknowledgement

The authors thank Anshul Chawla, David C. Morse and Timothy P. Lodge for useful discussions. This work was supported by NSF DMR-1719692. Computational resources were provided from Minnesota Supercomputing Institute (MSI) and UMN MRSEC through DMR-2011401.

# **Supporting Information**

Monte Carlo constants; fitting coefficients for the modified RPA; comparison to Fig. 2 of Ref. 31, SCFT calculation of the ODT; structure factors and simulation snapshots for other values of  $\chi N$ ; structure factors for defective crystallization at  $\epsilon = 1$ ; structure factors for defect-free crystallization at  $\epsilon = 3$ ; snapshots of crystallization at  $\epsilon = 1$  for L = 1.86; snapshots of the absence of melting for  $\epsilon = 3$  for L = 7.22; SCFT volume fractions for bcc on the [111] direction

### References

- (1) Matsen, M. W.; Bates, F. S. Unifying weak- and strong-segregation block copolymer theories. *Macromolecules* **1996**, *29*, 1091–1098.
- (2) Matsen, M. W.; Schick, M. Stable and unstable phases of a diblock copolymer melt. *Phys. Rev. Lett.* **1994**, *72*, 2660–2663.
- (3) Huang, Y. Y.; Hsu, J. Y.; Chen, H. L.; Hashimoto, T. Existence of fcc-packed spherical micelles in diblock copolymer melt. *Macromolecules* **2007**, *40*, 406–409.

- (4) Hsu, N. W.; Nouri, B.; Chen, L. T.; Chen, H. L. Hexagonal Close-Packed Sphere Phase of Conformationally Symmetric Block Copolymer. *Macromolecules* 2020, 53, 9665– 9675.
- (5) Frank, F. C.; Kasper, J. S. Complex alloy structures regarded as sphere packings. I. Definitions and basic principles. Acta Crystallogr. 1958, 11, 184–190.
- (6) Frank, F. C.; Kasper, J. S. Complex alloy structures regarded as sphere packings. II. Analysis and classification of representative structures. Acta Crystallogr. 1959, 12, 483–499.
- (7) Lee, S.; Bluemle, M. J.; Bates, F. S. Discovery of a Frank-Kasper  $\sigma$  phase in sphere-forming diblock copolymer melts. *Science* **2010**, *330*, 349–353.
- (8) Lee, S.; Leighton, C.; Bates, F. S. Sphericity and symmetry breaking in the formation of Frank-Kasper phases from one component materials. *Proc. Natl. Acad. Sci. USA* 2014, 111, 17723–17731.
- (9) Gillard, T. M.; Lee, S.; Bates, F. S. Dodecagonal quasicrystalline order in a diblock copolymer melt. *Proc. Natl. Acad. Sci. USA* **2016**, *113*, 5167–5172.
- (10) Bates, M. W.; Lequieu, J.; Barbon, S. M.; Lewis III, R. M.; Delaney, K. T.; Anastasaki, A.; Hawker, C. J.; Fredrickson, G. H.; Bates, C. M. Stability of the A15 phase in diblock copolymer melts. *Proc. Natl. Acad. Sci. USA* 2019, 116, 13194–13199.
- (11) Bates, M. W.; Barbon, S. M.; Levi, A. E.; Lewis III, R. M.; Beech, H. K.; Vonk, K. M.; Zhang, C.; Fredrickson, G. H.; Hawker, C. J.; Bates, C. M. Synthesis and Self-Assembly of AB<sub>n</sub> miktoarm star polymers. ACS Macro Lett. 2020, 9, 396–403.
- (12) Jeon, S.; Jun, T.; Jo, S.; Ahn, H.; Lee, S.; Lee, B.; Ryu, D. Y. Frank-Kasper phases identified in PDMS-b-PTFEA copolymers with high conformational asymmetry. *Macromol. Rapid Commun.* **2019**, *40*, 1900259.

- (13) Schulze, M. W.; Lewis III, R. M.; Lettow, J. H.; Hickey, R. J.; Gillard, T. M.; Hillmyer, M. A.; Bates, F. S. Conformational asymmetry and quasicrystal approximants in linear diblock copolymers. *Phys. Rev. Lett.* **2017**, *118*, 207801.
- (14) Mueller, A. J.; Lindsay, A. P.; Jayaraman, A.; Lodge, T. P.; Mahanthappa, M. K.; Bates, F. S. Quasicrystals and Their Approximants in a Crystalline-Amorphous Diblock Copolymer. *Macromolecules* 2021, 54, 2647–2660.
- (15) Lindsay, A. P.; Jayaraman, A.; Peterson, A. J.; Mueller, A. J.; Weigand, S.; Mahanthappa, M. K.; Lodge, T. P.; Bates, F. S. Reevaluation of Poly(ethylene-alt-propylene)-block-Polydimethylsiloxane Phase Behavior Uncovers Topological Close-Packing and Epitaxial Quasicrystal Growth. ACS Nano 2021, 15, 9453–9468.
- (16) Kim, K.; Schulze, M. W.; Arora, A.; Lewis III, R. M.; Hillmyer, M. A.; Dorfman, K. D.; Bates, F. S. Thermal processing of diblock copolymer melts mimics metallurgy. *Science* 2017, 356, 520–523.
- (17) Kim, K.; Arora, A.; Lewis III, R. M.; Liu, M.; Li, W.; Shi, A.-C.; Dorfman, K. D.; Bates, F. S. Origins of low-symmetry phases in asymmetric diblock copolymer melts. *Proc. Natl. Acad. Sci. USA* 2018, 115, 847–854.
- (18) Xie, N.; Li, W.; Qiu, F.; Shi, A.-C.  $\sigma$  phase formed in conformationally asymmetric AB-type block copolymers. *ACS Macro Lett.* **2014**, *3*, 906–910.
- (19) Grason, G. M.; DiDonna, B. A.; Kamien, R. D. Geometric theory of diblock copolymer phases. *Phys. Rev. Lett.* **2003**, *91*, 058304.
- (20) Grason, G. M. The packing of soft materials: Molecular asymmetry, geometric frustration and optimal lattices in block copolymer melts. *Phys. Rep.* **2006**, *433*, 1–64.
- (21) Reddy, A.; Buckley, M. B.; Arora, A.; Bates, F. S.; Dorfman, K. D.; Grason, G. M.

- Stable Frank-Kasper phases of self-assembled, soft matter spheres. *Proc. Natl. Acad. Sci. USA* **2018**, *115*, 10233–10238.
- (22) Milner, S. T. Chain Architecture and Asymmetry in Copolymer Microphases. *Macro-molecules* **1994**, *27*, 2333–2335.
- (23) Bates, F. S.; Fredrickson, G. H. Conformational asymmetry and polymer-polymer thermodynamics. *Macromolecules* **1994**, *27*, 1065–1067.
- (24) Matsen, M. W.; Bates, F. S. Conformationally asymmetric block copolymers. *J. Polym. Sci. B Polym. Phys.* **1997**, *35*, 945–952.
- (25) Fredrickson, G. H.; Helfand, E. Fluctuation effects in the theory of microphase separation in block copolymers. *J. Chem. Phys.* **1987**, *87*, 697–705.
- (26) Lewis III, R. M.; Arora, A.; Beech, H. K.; Lee, B.; Lindsay, A. P.; Lodge, T. P.; Dorfman, K. D.; Bates, F. S. Role of chain length in the formation of Frank-Kasper phases in diblock copolymers. *Phys. Rev. Lett.* 2018, 121, 208002.
- (27) Wang, J.; Wang, Z.-G.; Yang, Y. Nature of Disordered Micelles in Sphere-Forming Block Copolymer Melts. *Macromolecules* **2005**, *38*, 1979–1988.
- (28) Ghasimakbari, T.; Morse, D. C. Correlations in Disordered Melts of Asymmetric Diblock Copolymers. *Macromolecules* **2018**, *51*, 2335–2348.
- (29) Duchs, D.; Ganesan, V.; Fredrickson, G. H.; Schmid, F. Fluctuation Effects in Ternary AB + A + B Polymeric Emulsions. *Macromolecules* **2003**, *36*, 9237–9248.
- (30) Stasiak, P.; Matsen, M. W. Monte Carlo Field-Theoretic Simulations for Melts of Symmetric Diblock Copolymer. *Macromolecules* **2013**, *46*, 8037–8045.
- (31) Vorselaars, B.; Stasiak, P.; Matsen, M. W. Field-Theoretic Simulation of Block Copolymers at Experimentally Relevant Molecular Weights. *Macromolecules* **2015**, *48*, 9071–9080.

- (32) Spencer, R. K. W.; Vorselaars, B.; Matsen, M. W. Continuous Thermodynamic Integration in Field-Theoretic Simulations of Structured Polymers. *Macromol. Theory Simul.* **2017**, *26*, 1700036.
- (33) Beardsley, T. M.; Spencer, R. K. W.; Matsen, M. W. Computationally Efficient Field-Theoretic Simulations for Block Copolymer Melts. *Macromolecules* 2019, 52, 8840–8848.
- (34) Beardsley, T. M.; Matsen, M. W. Fluctuation correction for the order-disorder transition of diblock copolymer melts. *J. Chem. Phys.* **2021**, *154*, 124902.
- (35) Fredrickson, G. H. *The Equilibrium Theory of Inhomogeneous Polymers*; Oxford University Press: Oxford, 2006.
- (36) Fredrickson, G. H.; Ganesan, V.; Drolet, F. Field-Theoretic Computer Simulation Methods for Polymers and Complex Fluids. *Macromolecules* **2002**, *35*, 16–39.
- (37) Delaney, K. T.; Fredrickson, G. H. Recent Developments in Fully Fluctuating Field-Theoretic Simulations of Polymer Melts and Solutions. J. Phys. Chem. B 2016, 120, 7615–7634.
- (38) Cheong, G. K.; Chawla, A.; Morse, D. C.; Dorfman, K. D. Open-source code for self-consistent field theory calculations of block polymer phase behavior on graphics processing units. *Eur. Phys. J. E* **2020**, *43*, 15.
- (39) Stasiak, P.; Matsen, M. W. Efficiency of pseudo-spectral algorithms with Anderson mixing for the SCFT of periodic block-copolymer phases. *Eur. Phys. J. E* **2011**, *34*, 110.
- (40) Olvera de la Cruz, M.; Edwards, S. F.; Sanchez, I. C. Concentration fluctuations in polymer blend thermodynamics. *J. Chem. Phys.* **1988**, *89*, 1704–1708.

- (41) Morse, D. C.; Qin, J. Relationships among coarse-grained field theories of fluctuations in polymer liquids. *J. Chem. Phys.* **2011**, *134*, 084902.
- (42) Eitouni, H. B.; Balsara, N. P.; Hahn, H.; Pople, J. A.; Hempenius, M. A. Ther-modynamic Interactions in Organometallic Block Copolymers: Poly(styrene-block-ferrocenyldimethylsilane). *Macromolecules* 2002, 35, 7765–7772.
- (43) Leibler, L. Theory of microphase separation in block copolymers. Macromolecules 1980, 13, 1602–1617.
- (44) Schwab, M.; Stuhn, B. Thermotropic Transition from a State of Liquid Order to a Macrolattice in Asymmetric Diblock Copolymers. *Phys. Rev. Lett.* **1996**, *76*, 924–927.
- (45) Chawla, A.; Bates, F. S.; Dorfman, K. D.; Morse, D. C. Structure in Disordered Sphere-Forming Diblock Copolymer Melts. *Phys. Rev. Mater.* **2021**, *5*, L092601.
- (46) Dormitontova, E. E.; Lodge, T. P. The Order-Disorder Transition and the Disordered Micelle Regime in Sphere-Forming Block Copolymer Melts. *Macromolecules* 2001, 34, 9143–9155.
- (47) Ghasimakbari, T.; Morse, D. C. Order-Disorder Transitions and Free Energies in Asymmetric Diblock Copolymers. *Macromolecules* **2020**, *53*, 7399–7409.
- (48) Vavasour, J. D.; Whitmore, M. D. Self-consistent field theory of block copolymers with conformational asymmetry. *Macromolecules* **1993**, *26*, 7070–7075.
- (49) Matsen, M. W.; Beardsley, T. M. Field-theoretic simulations for block copolymer melts using the partial saddle-point approximation. *Polymers (Basel)*. **2021**, *13*, 2437.
- (50) Mysona, J. A.; McCormick, A. V.; Morse, D. C. Simulation of diblock copolymer surfactants. I. Micelle free energies. *Phys. Rev. E* **2019**, *100*, 012602.
- (51) Tyler, C. A.; Morse, D. C. Stress in self-consistent field theory. *Macromolecules* **2003**, 36, 8184–8188.